Ultrasonics 65 (2016) 87–95

Contents lists available at ScienceDirect

Ultrasonics

journal homepage: www.elsevier.com/locate/ultras

Combination of nonlinear ultrasonics and guided wave tomography for imaging the micro-defects

Weibin Li [a], Younho Cho [b,*]

[a] Department of Aeronautics, Xiamen University, 422, South Siming Road, 361005 Xiamen, China
[b] School of Mechanical Engineering, Pusan National University, 10511, San 30, Jangjeon-dong, Geumjeong-gu, 609-735 Busan, South Korea

ARTICLE INFO

Article history:
Received 25 January 2015
Received in revised form 12 October 2015
Accepted 16 October 2015
Available online 30 October 2015

Keywords:
Nonlinearity
Imaging
Rayleigh surface waves
Micro-defects

ABSTRACT

The use of guided wave tomography has become an attractive alternative to convert ultrasonic wave raw data to visualized results for quantitative signal interpretation. For more accurate life prediction and efficient management strategies for critical structural components, there is a demand of imaging micro-damages in early stage. However, there is rarely investigation on guided wave tomographic imaging of micro-defects. One of the reasons for this might be that it becomes challenging to monitor tiny signal difference coefficient in a reliable manner for wave propagation in the specimens with micro-damages. Nonlinear acoustic signal whose frequency differs from that of the input signal can be found in the specimens with micro-damages. Therefore, the combination of guided wave tomography and nonlinear acoustic response induced by micro-damages could be a feasibility study for imaging micro-damages. In this paper, the nonlinear Rayleigh surface wave tomographic method is investigated to locate and size micro-corrosive defect region in an isotropic solid media. The variations of acoustic nonlinear responses of ultrasonic waves in the specimens with and without defects are used in guided wave tomographic algorithm to construct the images. The comparisons between images obtained by experimental signals and real defect region induced by hydrogen corrosion are presented in this paper. Results show that the images of defect regions with different shape, size and location are successfully obtained by this novel technique, while there is no visualized result constructed by conventional linear ultrasonic tomographic one. The present approach shows a potential for inspecting, locating and imaging micro-defects by nonlinear Rayleigh surface wave tomography.

1. Introduction

The use of nonlinear ultrasonic waves has been proposed as a potential method for detecting micro-defects to which linear ultrasonic methods are less sensitive [1–4]. Recently, nonlinear ultrasonic approaches have been reported in numerous studies to assess material micro-damage [5,6] and characterize material degradation [7,8], respectively. Since the energy of Rayleigh surface waves is concentrated near the surface, these waves are taken as an efficient tool for non-destructive evaluation (NDE) of damages that initiates at the material surface [9]. Additional advantages of Rayleigh surface waves include longer propagation distance than for conventional bulk waves to interrogate large, complex components where is not accessible for visual inspection. Considering the high sensitivity of nonlinear ultrasonic method and the great advantages of surface guided wave approach, nonlinear ultrasonic surface wave technique has drawn significant attention for nondestructive evaluation of damages in early stages [10–12].

Another remarkable progress of ultrasonic wave NDE is an imaging potential over a hidden or inaccessible damage zone. One of the effective ways to quantitatively monitor a structure is to obtain the images via either scanning or tomography [13]. There have been a number of different tomographic schemes, and some of the most well-known methods are time-difference-of-arrival imaging method, energy arrival and the reconstruction algorithm for the probabilistic inspection of damage (RAPID) method [14–16]. The RAPID based tomographic approach is apt to be implemented efficiently with ultrasonic guided wave features. The major advantage of using RAPID algorithm is the simplicity in the data interpretation, that the wave diffraction is accounted only on the line of propagation path with the linear interpolation of defect location probability distribution [17]. However, to authors' knowledge, most of earlier efforts of guided wave tomographic techniques have been limited to the use of linear features

* Corresponding author.
E-mail address: mechcyh@pusan.ac.kr (Y. Cho).

http://dx.doi.org/10.1016/j.ultras.2015.10.016
0041-624X/

of time domain wave signals for imaging macro-damages. There is rarely investigation on nonlinear guided wave tomographic imaging of micro-defects. One of the reasons for this might be that it becomes challenging to monitor tiny signal difference coefficient in a reliable manner for wave propagation in the specimens with micro-damages. Recently, Solodov and Busse [18] reported the application of local defect resonance concept enhances substantially the efficiency of vibro-thermal conversion in ultrasonic thermography for resonance ultrasonic thermography for imaging contact crack. Solodov and Busse [19] and Eren et al. [20] developed experimental methodologies of nonlinear scanning laser vibrometry and nonlinear air-coupled emission to study the interactions of nonlinear elastic wave and defects for defect-selective imaging of closed cracks. It has verified the higher sensitivity and resolution of imaging micro-damages by acoustic nonlinear response [21].

In this paper, nonlinear Rayleigh surface wave tomographic technique, is investigated to locate and size micro-corrosive defect region in an isotropic solid media. Instead of extracting the linear features from a time domain wave signal, the nonlinear acoustic signal in frequency domain which caused by the frequency conversion of Rayleigh surface wave signals is used in the modified tomographic algorithm. Nonlinear parameter of Rayleigh surface wave propagation in an isotropic medium is derived to express the nonlinear feature of surface waves. A modified RAPID tomographic algorithm is developed to construct the images of various defects in aluminum plates. The tomographic images of artificial chemical corrosive defect regions in the specimens are reconstructed by combining acoustic nonlinear response with the modified guided wave tomography. The proposed technique shows a potential for inspecting, locating and imaging micro-defects by nonlinear Rayleigh surface wave tomography.

2. Theory

2.1. Nonlinear surface wave

Rayleigh surface wave propagates in a positive x direction, while z axis points into the half-space as shown in Fig. 1. According to partial wave techniques, the displacement of Rayleigh surface wave propagating in an isotropic half-space with traction-free boundary condition could be decomposed into in-plane and out-of-plane contributions [9,10,12,22–24].

The displacement potentials that describe the longitudinal and shear waves are written as,

$$u = \frac{\partial \phi}{\partial x} - \frac{\partial \varphi}{\partial z}, \tag{1}$$

$$w = \frac{\partial \phi}{\partial z} + \frac{\partial \varphi}{\partial x}, \tag{2}$$

$$\phi = \frac{A}{ik} e^{-pz} e^{i(kx-wt)}, \tag{3}$$

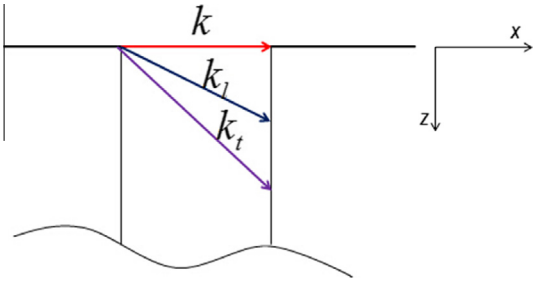

Fig. 1. Surface wave propagation along x direction.

$$\varphi = \frac{B}{ik} e^{-qz} e^{i(kx-wt)}, \tag{4}$$

where $p^2 = k^2 - k_l^2$, $q^2 = k^2 - k_t^2$, and k, k_l and k_t are the wave number for surface wave, longitudinal wave and transverse wave, respectively. w is angle frequency. The stress free boundary conditions demand that the stresses σ_{zz} and σ_{xz} go to zero on the surface ($z = 0$). The constants A and B are related by

$$B = -iA\frac{2kp}{k^2 + q^2}. \tag{5}$$

Partial wave technique and normal modal expanding method are used to analyze the amplitude relation of fundamental wave and second harmonic wave displacement [22,25]. On the surface, the Rayleigh surface wave can be decomposed into the cross-interaction and self-interaction of longitudinal and shear wave components. So the displacement components of fundamental frequency wave and second harmonic surface waves on the surface can be represented as

$$u(f) = A\left(e^{-pz} - \frac{2pq}{k^2 + q^2} e^{-qz}\right) e^{i(kx-wt)}, \tag{6}$$

$$w(f) = iA\frac{p}{k}\left(e^{-pz} - \frac{2k^2}{k^2 + q^2} e^{-qz}\right) e^{i(kx-wt)}, \tag{7}$$

$$u(2f) = D\left(e^{-2pz} - \frac{2pq}{k^2 + q^2} e^{-2qz}\right) e^{-i2wt}, \tag{8}$$

$$w(2f) = iD\frac{p}{k}\left(e^{-2pz} - \frac{2k^2}{k^2 + q^2} e^{-2qz}\right) e^{-i2wt}. \tag{9}$$

The second harmonic field can be described as,

$$D = \sum_{n=1}^{3} C^{(n)} e^{ik^{(n)}x}, \tag{10}$$

where

$$C^{(1)} = -\left(\frac{3\rho c_l^2 + C_{111}}{8\rho c_l^2}\right) k_l^2 A^2 x, \quad k^{(1)} = 2k_l. \tag{11}$$

$$C^{(2)} = -\left(\frac{\rho c_l^2 + C_{166}}{4\rho c_l^2}\right) \frac{k_t^3 A^2}{(k_t^2 - k_l^2)} \sin[(k_t - k_l)x], \quad k^{(2)} = k_l + k_t. \tag{12}$$

$$C^{(3)} = -\left(\frac{\rho c_l^2 + C_{166}}{\rho c_t^2}\right) \frac{(k_l k_t^2 + k_t k_l^2) A^2}{(k_l + k_t)^2 - 4k_t^2} \sin\left[\left(\frac{k_t - k_l}{2}\right)x\right],$$
$$k^{(3)} = \frac{3k_t + k_l}{2}. \tag{13}$$

It is found that $C^{(2)}$ and $C^{(3)}$ will vanish at a certain propagation distance, which means these two components have no accumulative contributions to second harmonic Rayleigh surface wave filed. It assumed that wave propagation distance is sufficiently long, so the second harmonic field could be mainly attributed to $C^{(1)}$. From above analysis, it is found that the relationship between D and A on the surface can be expressed as

$$D = \frac{\beta_l k_l^2 A^2 x}{8} e^{i2kx}, \tag{14}$$

where $\beta_l = -\frac{3\rho c_l^2 + C_{111}}{8\rho c_l^2}$ is the acoustic nonlinearity parameter for longitudinal wave; x is wave propagation distance. The similar results can also be found in [10]. Generally, the out-of-plane displacement

is easier to be detected experimentally, so in this investigation, we use out-of-plane displacement to calculate the nonlinear parameter of surface wave. After submitting Eq. (14) into Eq. (9), it could find the relation of surface wave nonlinear parameter expressed by the out-of-plane displacements amplitude at the surface ($z = 0$) as

$$\beta = \frac{w(2f)}{w^2(f)} \frac{8i}{k_l^2 x} \frac{p}{k} \left(1 - \frac{2k^2}{k^2 + q^2}\right). \tag{15}$$

If we consider the attenuation factor, the acoustic nonlinear parameter can be modified by the attenuation correction factor as

$$D_\alpha = \left(\frac{m}{1 - e^{-m}}\right), \; m = (\alpha_2 - 2\alpha_1)x, \tag{16}$$

where α_1 and α_2 are the attenuation coefficient of fundamental wave and second harmonic wave, respectively. So nonlinear parameters of surface wave can be modified as

$$\beta = \frac{A_2}{A_1^2} \frac{8i}{k_l^2 x} \frac{p}{k} \left(1 - \frac{2k^2}{k^2 + q^2}\right) D_\alpha, \tag{17}$$

where A_1 and A_2 are the out-of-plane displacement amplitude of fundamental and second harmonic wave, respectively. It is found that the ratios of the amplitudes of the second harmonic and the fundamental wave grow with the propagation distance via the accumulative effect to a certain point that material attenuation becomes dominant [7,10,11].

2.2. Modified tomographic algorithm

The principle for the guided wave tomographic approach is shown in Fig. 2. The probabilistic approach known as reconstructive algorithm for probabilistic inspection of damage consists of signal comparison and image reconstruction [26]. The signal comparison part is based upon a damage index named signal difference coefficient (SDC), which is a measure of how statistically different the signal in specimen with defect is from a reference one in that without defect. Damage indexes for all transducer pairs are spatially distributed and summed to generate an image of the damage area [14,15]. The first step of this algorithm is the computation of the SDC between the signal $x_{ij}(t)$ and the baseline $y_{ij}(t)$, which is the drop in the correlation coefficient over a specified time window. The index i denotes the transmitter and j corresponds to the receiver, respectively. As mathematical formulation, SDC can be stated as,

$$\mathrm{SDC}_{ij} = 1 - \left| \frac{\int_{t_0}^{t_0+\Delta T} [x_{ij}(t) - \mu][y_{ij}(t) - \mu] dt}{\sqrt{\int_{t_0}^{t_0+\Delta T} [x_{ij}(t) - \mu]^2 dt \int_{t_0}^{t_0+\Delta T} [y_{ij}(t) - \mu]^2 dt}} \right|, \tag{18}$$

where time t_0 is the direct arrival time for each transducer pair; μ is the mean of the corresponding signal, and Δt is a time window. If the signals are identical, the SDC is zero and if the signals are completely out of phase, the SDC will achieve its maximum value of 1.

After the SDC value for all sensor pairs are calculated, the next step of RAPID algorithm is image reconstruction. Images are generated by spatially distributing each SDC value in an elliptical pattern. A parameter γ is defined to control the size of the ellipse [17]. The amplitude tapers from its maximum value along the line connecting the ellipse foci to zero on the periphery of the ellipse. Note that parameter γ is the shape factor that controls the size of the elliptical distribution. This value of this parameter is greater than 1.0. The spatial distribution function, in which SDC values will distribute in the final step of the algorithm, defined as,

$$s_{ij}(x, y) = \frac{\gamma - R_{ij}(x, y)}{1 - \gamma}, \quad \text{for } \gamma > R_{ij}(x, y), \tag{19}$$

$$s_{ij}(x, y) = 0, \quad \text{otherwise}, \tag{20}$$

where $R_{ij}(x, y)$ is the ratio of the sum of distances of the point (x, y) to the transmitter i and receiver j to the distance between the transmitter and receiver and is mathematically stated as

$$R_{ij}(x, y) = \frac{\sqrt{(x_i - x)^2 + (y_i - y)^2} + \sqrt{(x_j - x)^2 + (y_j - y)^2}}{\sqrt{(x_i - x_j)^2 + (y_i - y_j)^2}}. \tag{21}$$

In the conventional RAPID algorithm, the shape factor is merely greater than 1. This guideline is not sufficient to estimate a defect area [17,26]. However, if we know the approximate distance of the defect zone on transmitter–receiver pair, the shape factor γ can be calculated by using Eq. (21). Fig. 3 shows the schematic of the calculation of the shape factor.

If all of the distances of the defect region are the same of the transmitter–receiver pairs, γ will be a uniform number. But distances of the defect range will not equal that of the

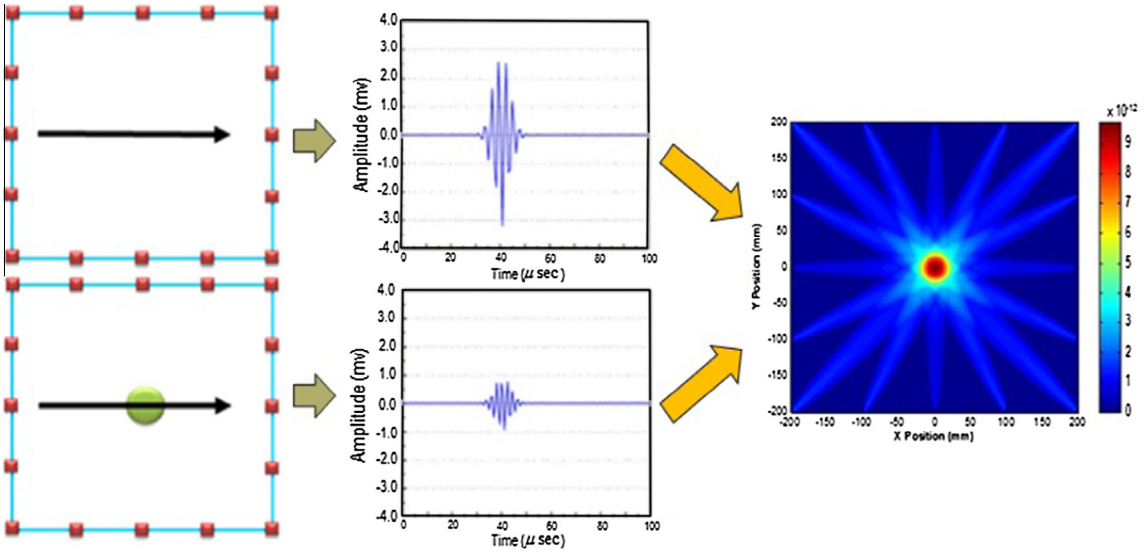

Fig. 2. Principle of guided wave tomography based on SDC.

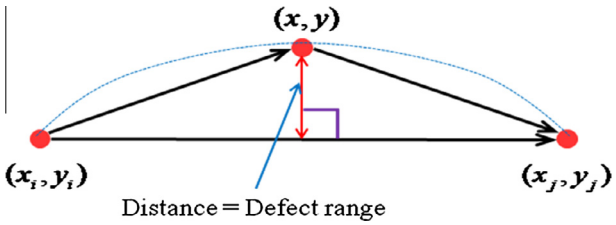

Fig. 3. Schematic of calculation of a shape factor.

transmitter–receiver pairs, so the value of γ will vary. The shape factor γ is related transmitter–receiver pairs, so Eq. (19) has to be corrected as below.

$$s_{ij}(x,y) = \frac{\gamma_N - R_{ij}(x,y)}{1-\gamma_N}, \quad \text{for } \gamma_N > R_{ij}(x,y), \tag{22}$$

where N is the total number of transmitter–receiver pairs. Finally, the image amplitude at each pixel is the linear summation of the location probabilities from each transmitter–receiver pair with the total number of transmitter–receiver pairs given by N and is stated as,

$$P(x,y) = \sum_{i=1}^{N-1}\sum_{j=i+1}^{N} \mathrm{SDC}_{ij} s_{ij}(x,y). \tag{23}$$

3. Experiment

The specimens under investigation are rectangular aluminum plates with dimensions of 500 mm × 500 mm and the thickness is 10 mm. As shown in Fig. 4, each specimen contains one artificial chemical corrosive region. The location, shape and dimensions of the corrosive region are shown in Fig. 4.

The schematic diagram of the measurement is illustrated in Fig. 5. A high-power tone burst system with a pair of narrow band transducers is employed to generate a narrow band signal with a central frequency of 1 MHz. The attenuator and receiver unit are equipped with an amplifier connected to the transducers. For nonlinear ultrasonic measurement, while the input frequency is tuned at 1 MHz, the central frequency of the receiver is chosen at 2 MHz to obtain the second harmonic frequency components. Wave velocity of Rayleigh surface wave in this specimens is 2.795 km/s. The incident angle is designed to launch Rayleigh wave mode into the specimen by Snell's law. The transducers are mounted on the specimen with couplant. The waveforms are digitally processed using the fast Fourier transformation (FFT) to obtain the frequency spectrogram to check the primary wave amplitude A_1 at the fundamental frequency, and second harmonic amplitude A_2 at the double frequency, respectively.

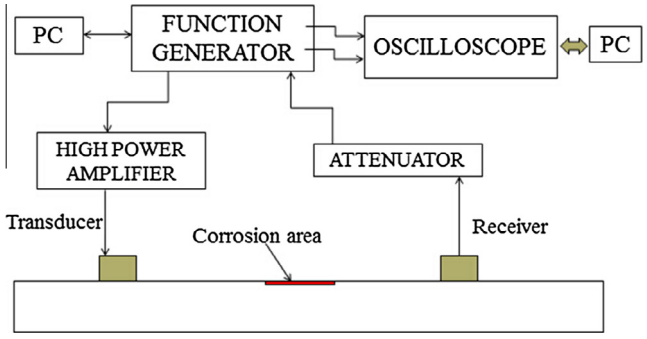

Fig. 5. Block diagram of ultrasonic measurement system.

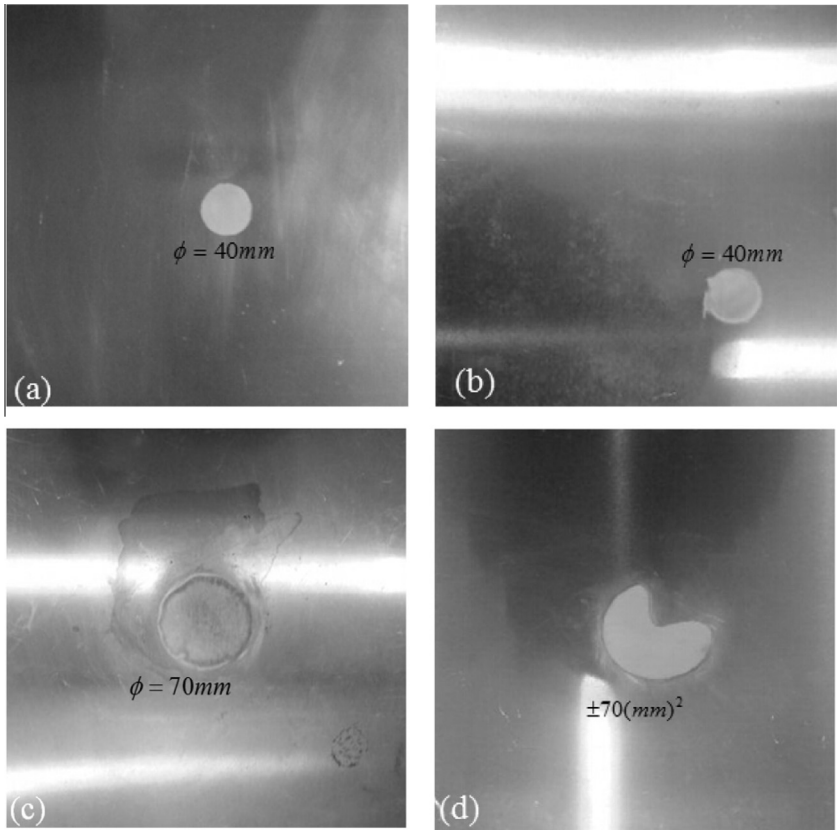

Fig. 4. The specimens with different defects.

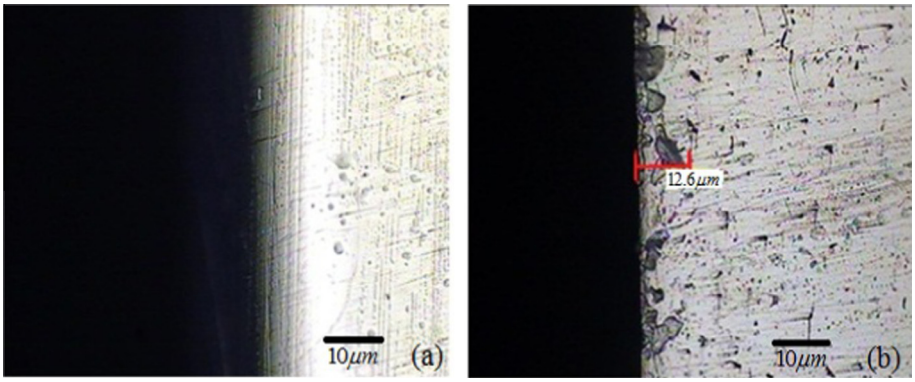

Fig. 6. Specimens without (a) and with (b) chemical corrosion on the surface.

The physical effect of nonlinear ultrasonic test is the measurement of acoustic signal whose frequency differs from that of the input signal. Generally, the formation of nonlinear acoustic signal at different frequency of the fundamental input frequency, results from waveform distortion of ultrasonic signal propagation in the specimen with nonlinearity sources. Surface waves are very sensitive to the surface conditions of tested specimens, like residual stress, roughness, oxidization and so on. In this study, the artificial chemical corrosive defects are introduced into the specimens. The hydrogen corrosion used in this work, is a form of metal corrosion occurring in the presence of acidic condition, which involves a redox reaction that reduces hydrogen ions, forming molecular hydrogen [27]. When hydrochloric acid is employed on the surface of specimen, anodic dissolution at the exposed surface leads to crack initiation and propagation [28]. The chemical corrosion can be concentrated locally to form micro-pits or micro-cracks. For further confirmation of the initiation of micro-defects after chemical corrosion at the surface of specimen, micro-structural pictures are shown in Fig. 6. The pictures show the apparent micro-pits and cavities by chemical corrosion. The distributed micro-defects are the main source of nonlinearity. The acoustic nonlinearity is increased significantly by the formation of micro-cracks that cause contact nonlinearity, with increased initiation and propagation of the micro-cracks.

4. Results and discussions

4.1. Image reconstructed by linear time domain signals

The ultrasonic surface wave pulse–echo method is used to preliminary estimate the interpolation parameter of the defect region. In the subsequent process, the pitch–catch based RAPID algorithm is employed in the same corresponding positions of the transmitter and receiver as the ones for the preliminary pulse–echo test. As discussed in Section 2, in conventional tomographic algorithm, the value of signal difference coefficient (SDC) is calculated by the variations of linear feature of wave signals due to the scattering, reflecting, refracting of guided waves with defects. So the defect size should be comparable with the wavelength of ultrasonic waves.

In this work, linear guided waves based tomographic approach is firstly employed to generate the images of micro-corrosive

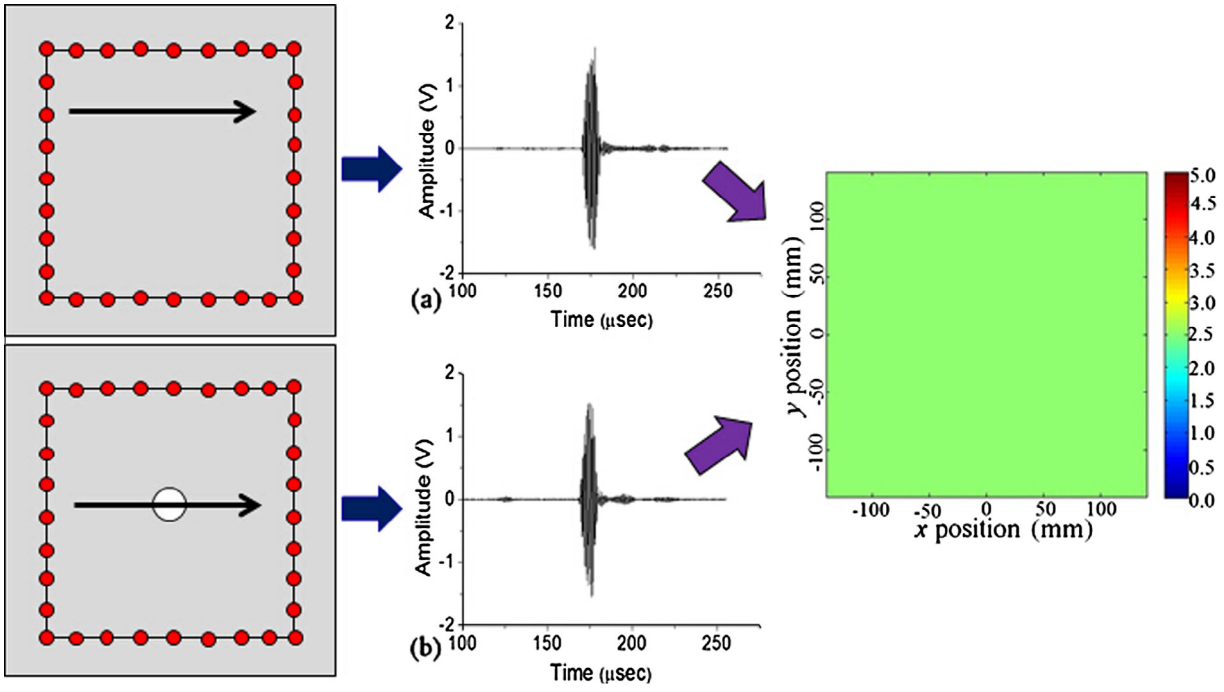

Fig. 7. Conventional ultrasonic tomography based on linear time domain signals.

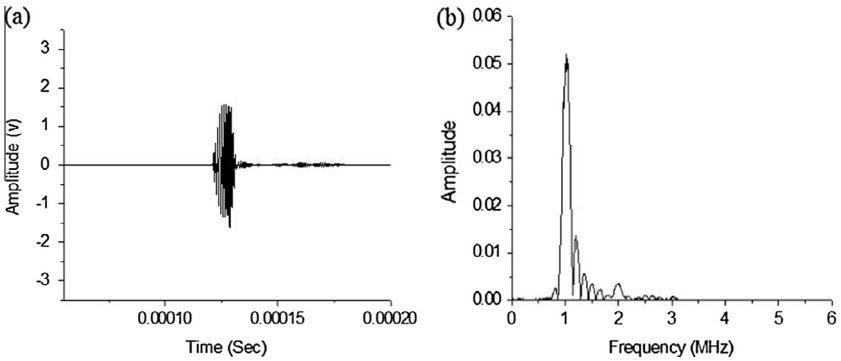

Fig. 8. Typical received signal: (a) time domain signal, and (b) frequency spectra of the fundamental and second harmonic signal.

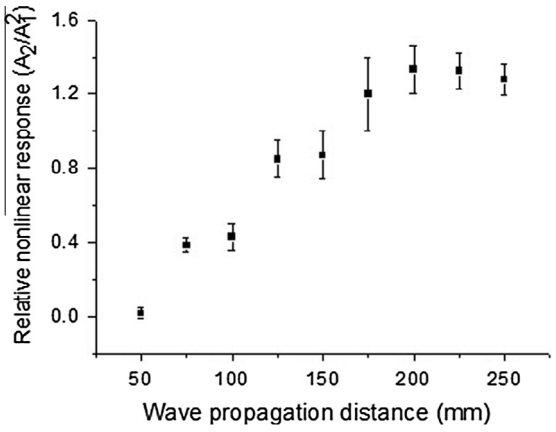

Fig. 9. Cumulative effect of nonlinear response as propagation distance.

defects. As shown in Fig. 7, it is hard to figure out any difference between the linear time domain signals that propagate through the regions with and without tiny chemical corrosive defects. The value of calculated SDC approximately equals zero when the linear time domain signal is employed in conventional tomography algorithm. So, tomographic image by conventional linear time domain signals could not present any information of micro-corrosive defects.

4.2. Nonlinearity measurement

The sensitivity of nonlinear ultrasonic methods to the damages features is far greater than that of linear acoustic approach. Measured nonlinearity should include damage-induced nonlinearity plus any nonlinearity from instrumentations and couplant. To assure that the nonlinearity from material damage is dominated over other sources. Only the nonlinear parameters noticeable exceeding the baseline value of the raw specimens without damages after obtained over a number of times, and the average datas are plotted to alleviate the experimental uncertainly. A standard measurement is common to all four specimens, which ensure that the change of nonlinear parameter is the change of material inherent nonlinearity. Fig. 8 shows the typical waveform of a received signal and its frequency spectrum. The received time-domain

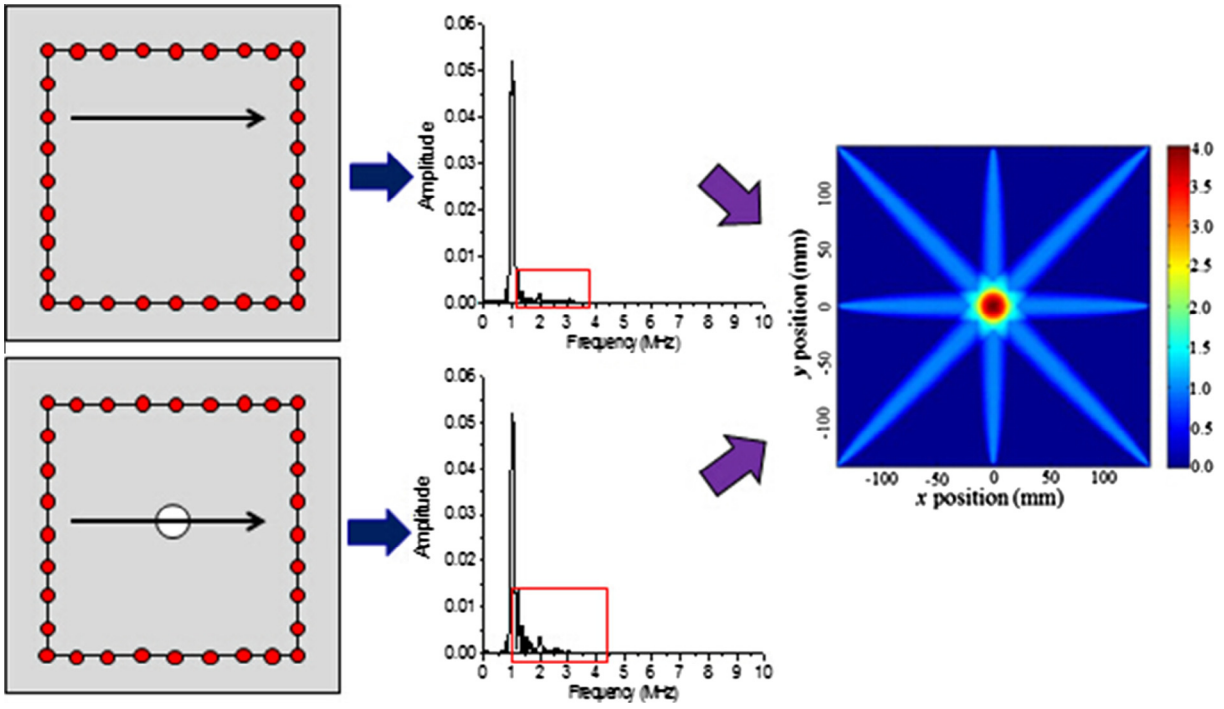

Fig. 10. Modified nonlinear ultrasonic tomographic image based on frequency domain signals.

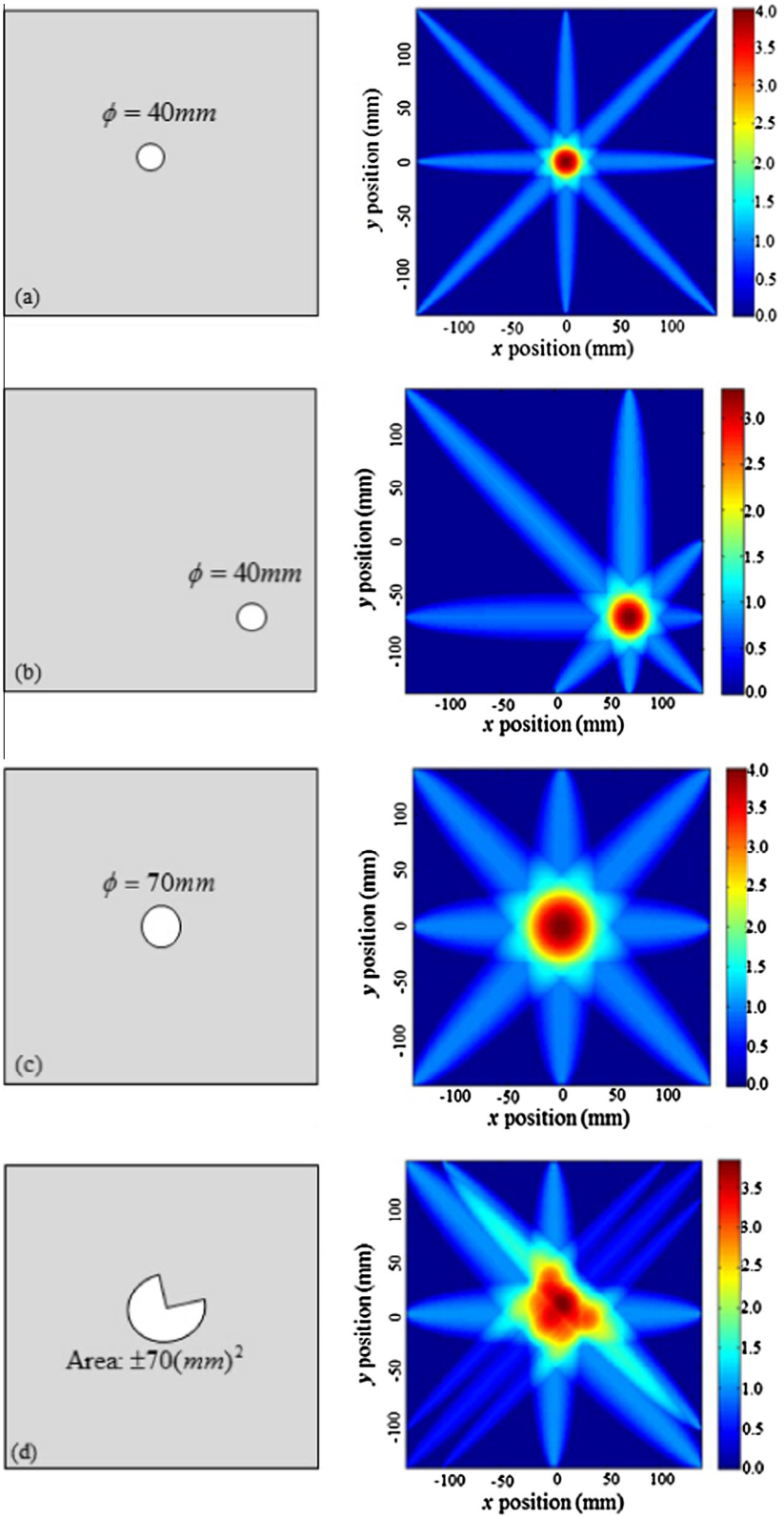

Fig. 11. Image of the defect region with different location, size and shape.

signal is processed in the frequency domain with the Fourier transform to obtain its spectrum.

The principal difference between linear and nonlinear ultrasonic test is that in the latter the existence and characteristics of defects are often related to an acoustic signal whose frequency differs from that of the input signal [7]. In this investigation, the frequency spectrum analysis to filter out the different frequency components is conducted. Nonlinear frequency components are used to calculate the SDC value in the tomographic algorithm.

For nonlinear guided wave test, nonlinear responses of higher harmonic generation which induced by instruments, coupling media as well as ambient noise are inevitable. However, the higher

harmonics induced by the material nonlinearity of specimen are the function of wave propagation distance as indicated in Eq. (17), but the harmonics induced by instrumental nonlinearity are not. When guided wave propagation distance increases, the value of second harmonics sources from setup or ambient noise remains consistent. Only the second harmonics sources from specimens can increase. The growth of second harmonic amplitude with propagation distance is called the cumulative effect [6,7]. To ensure that what is measured from the specimens is mainly due to the nonlinearity induced by the micro-damages rather than arising from the measurement system, demonstration of this cumulative effect is essential.

As expressed in Section 2.1, nonlinear response of Rayleigh surface wave is function of wave propagation distance, and can be modified by attenuation. To compare the experimental result of nonlinear parameter due to effect of acoustic nonlinearity of surface wave and theoretical derivation, experiments were conducted with respect to different propagation distance. Wave propagation distance was varied from 50 mm to 250 mm with 25 mm interval and conduct two times. The expression of the nonlinear parameter of Rayleigh surface waves show that, the parameter is defined as a function of frequency, material properties. In this work, since the same frequency surface wave mode is chosen to detect acoustic nonlinearity in the specimens with same materials, the influence of the feature function is neglected since the interest is focused on the variation of nonlinear response at certain frequency only. As shown in Fig. 9, it is found that the relative nonlinear parameter grows with the propagation distance via the accumulative effect to a certain point when material attenuation becomes dominant.

4.3. Images reconstructed by the nonlinear frequency components

As stated above, in the case of the scattering of an acoustic wave by the micro-crack, the amplitude of the nonlinear acoustic signals can be much greater than the level of those generated in intact media. Considering the nonlinear response of difference frequency components generation when the ultrasonic waves propagate through micro-damaged zone, the frequency domain signals are used to calculate the SDC value in this work. Thus, for nonlinear guided wave tomographic technique, instead of extracting the linear features from a time domain signal, frequency conversion induced by micro-damages of guided wave signals in frequency domain is used in the modified nonlinear tomographic algorithm.

The time domain Rayleigh surface wave signal was transformed into frequency spectrums to analyze the frequency conversion induced by micro-defect. Measured nonlinear acoustic signal in frequency domain was reconstructed by the modified RAPID algorithm to illustrate the tomographic image. Fig. 10 demonstrates the ability of the modified tomographic algorithm with the nonlinear surface wave signal to express the micro-defect region by image. The most significant variation in the SDC is observed approximately in the middle of the damage zone. There are also other zones of the tomogram that depict changes in the SDC that cannot be explained via a change in the material micro-defects in those zones. These anomalies includes the noise sources for the change in SDC include inconsistent sensor grounding, A/D jitter, and reproducibility of the gated sinusoid used to excite the sensors.

To ensure applicability to arbitrary shaped and located objects, the proposed technique is employed to image the micro-corrosive defect region with different size, location and shape in the specimens. The same experimental procedure is applied to measure the Rayleigh surface wave signal and launched along each path of sparse array network. As shown in Fig. 11, it is clearly illustrated that the present technique is readily used to reconstruct images of arbitrary shaped multiple defects with a satisfactory resolution and sensitivity in terms of size, shape and location of defect region.

It is important to note that the emphasis on this research is simply how changes in waveform distortion in specimens with different micro-damages translate into changes in tomograms. As shown in Fig. 11(b) and (d), if the defect is at the different location of the specimens, the wave propagation path in each direction is different. Therefore, the shape function for image reconstruction needs to be modified to illustrate the real defect [17,26]. The feasibility approach proposed in this investigation is to reconstruct the images of micro-defects by acoustic nonlinear response, while no visualized result constructed by conventional linear ultrasonic tomographic technique. Even some inevitable factors as mentioned above can result in the false color representation, the images of micro-corrosive defect regions in a qualitative manner are still obtained.

5. Conclusions

In this work, a nonlinear Rayleigh surface wave tomographic approach, is proposed to image, locate and size micro-corrosive region at the surface of aluminum plates. Nonlinear parameter of Rayleigh surface wave propagation in an isotropic medium is derived to express the nonlinear feature of surface waves. Instead of extracting the linear features from a time domain wave signal, the nonlinear Rayleigh surface wave signals in frequency domain is used in the modified tomographic algorithm to reconstruct the images. Image of micro-corrosive defect is successfully reconstructed by combining the acoustic nonlinear response with guided wave tomography, while no visualized result is obtained by conventional linear ultrasonic tomographic approach. The suggested method is applied to reconstruct the images of corrosive defect region with different size, location and shape. Results show that the modified nonlinear ultrasonic tomographic technique can be used for inspecting, locating and imaging micro-defects in solid media.

Acknowledgements

Authors would like to express our gratitude to professor J.D. Achenbach and professor Jianmin Qu from Northwestern University, USA for their invaluable advice and time to this work. This work was supported by the National Natural Science Fundation of China under Grant No: 51405405 and Fundamental Research Funds for the Central Universities under Grant No: 20720140511. This research was also supported by Research Program through the National Research Foundation of Korea (NRF) funded by the Ministry of Science, ICT & Future Planning (NRF-2015M2A2A9067474).

References

[1] W. Li, Y. Cho, J. Lee, J.D. Achenbach, Assessment of heat treated Inconel X-750 alloy by nonlinear ultrasonics, Exp. Mech. 53 (2013) 775–781.
[2] K.Y. Jhang, Application of nonlinear ultrasonics to the NDE of material degradation, IEEE Trans. Ultrason. Ferroelectr. Freq. Control 47 (2000) 540–548.
[3] J.H. Cantrell, W.T. Yost, Nonlinear ultrasonic characterization of fatigue microstructures, Int. J. Fatigue 23 (2001) 487–490.
[4] W. Li, S. Hyun, Y. Cho, Characterization of ultrasonic nonlinearity by thermal fatigue, Int. J. Precis. Eng. Man. 13 (2012) 935–940.
[5] S. Baby, B.N. Kowmudi, C.M. Omprakash, D.V.V. Statynarayana, K. Balasubramaniam, V. Kumar, Creep damage assessment in titanium alloy using a nonlinear ultrasonic technique, Scr. Mater. 59 (2008) 818–821.
[6] M. Deng, J. Pei, Assessment of accumulated fatigue damage in solid plates using nonlinear lamb wave approach, Appl. Phys. Lett. 90 (2007) 121902.
[7] W. Li, Y. Cho, J.D. Achenbach, Detection of thermal fatigue in composites by second harmonic Lamb waves, Smart Mater. Struct. 21 (2012) 085019.
[8] P.B. Nagy, Fatigue damage assessment by nonlinear ultrasonic material characterization, Ultrasonics 36 (1998) 375–381.

[9] G. Shui, J.Y. Kim, J. Qu, Y.S. Wang, L.J. Jacobs, A new technique for measuring the acoustic nonlinearity of materials using Rayleigh waves, NDT E Int. 41 (2008) 326–329.
[10] J. Herrmannn, J.Y. Kim, L.J. Jacobs, J. Qu, Assessment of material damage in a nickel-based superalloy using nonlinear Rayleigh surface waves, J. Appl. Phys. 99 (2006) 124913.
[11] M. Liu, J.Y. Kim, L.J. Jacobs, J. Qu, Experimental study of nonlinear Rayleigh wave propagation in shot-peened aluminium plates-feasibility of measuring residual stress, NDT E Int. 44 (2011) 67–74.
[12] H. Ogi, M. Hirao, S. Aoki, Noncontact monitoring of surface wave nonlinearity for predicting the remaining life of fatigued steels, J. Appl. Phys. 90 (2001) 438–442.
[13] K. Xu, D. Liu, D. Ta, B. Hu, W. Wang, Quantification of guided mode propagation in fractured long bones, Ultrasonics 54 (2014) 1210–1218.
[14] H. Gao, F. Yan, J.L. Rose, X. Zhao, Ultrasonic Guided Wave Tomography in Structural Health Monitoring of an Aging Aircraft Wing, The American Society for Nondestructive Testing, Columbus OH, 2005, pp. 412–415.
[15] J.K. Van Velsor, H. Gao, J.L. Rose, Guided-wave tomographic imaging of defects in pipe using a probabilistic reconstruction algorithm, Insight 49 (2007) 532–537.
[16] C.H. Wang, J.T. Rose, F. Chang, A synthetic time-reversal imaging method for structural health monitoring, Smart Mater. Struct. 13 (2004) 415–423.
[17] B. Sheen, Y. Cho, A study on quantitative lamb wave tomogram via modified RAPID algorithm with shape factor optimization, Int. J. Precis. Eng. Man. 16 (2012) 671–677.
[18] I. Solodov, G. Busse, Resonance ultrasonic thermography: highly efficient contact and air-coupled remote modes, Appl. Phys. Lett. 102 (2013) 061905.
[19] I. Solodov, G. Busse, Nonlinear air-coupled emission: the signature to reveal and image microdamage in solid materials, Appl. Phys. Lett. 91 (2007) 251910.
[20] E. Eren, S. Kurama, I. Solodov, Characterization of porosity and defect imaging in ceramic tile using ultrasonic inspections, Ceram. Int. 38 (2012) 2145–2151.
[21] N. Ichida, T. Sato, M. Linzer, Imaging the nonlinear ultrasonic parameter of medium, Ultrason. Imaging 5 (1983) 295–299.
[22] B.A. Auld, Acoustic Fields and Waves in Solids, Vols. I and Vols. II, Wiley, London, 1990.
[23] J.D. Achenbach, Wave Propagation in Elastic Solids, North-Holland Press, Amsterdam, 1973.
[24] Y. Shui, I.Y. Solodov, Nonlinear properties of Rayleigh and Stoneley waves in solids, J. Appl. Phys. 64 (1988) 6155–6165.
[25] M. Deng, Analysis of second-harmonic generation of Lamb wave modes using a modal analysis approach, J. Appl. Phys. 94 (2003) 4152–4159.
[26] W. Li, Y. Cho, Quantification and imaging of corrosion wall thinning using shear horizontal guided waves generated by magnetostrictive sensors, Sens. Actuators, A 232 (2015) 251–258.
[27] R.J. Gest, A.R. Troiano, Stress corrosion and hydrogen embrittlement in an aluminum alloy, Corrosion 30 (1974) 274–279.
[28] C.P. Jones, T.B. Scott, J.R. Petherbridge, J. Glascott, A surface science study of the initial stage of hydrogen corrosion on uranium metal and the role played by grain microstructure, Solid State Ionics 231 (2013) 81–86.